Research Article | Vol. 32, No. 27 / 30 Dec 2024 / Optics Express 48571
Optics EXPRESS

Quasi-ray tracing realization using a Bessel beam for optical alignment

ZHAOWEI CHEN,[1] ROBERT E. PARKS,[1,2] BHAWNA DHAWAN,[3] SURYA PRAKASH GURUNARAYANAN,[4] AND DAEWOOK KIM[1,*]

[1]James C. Wyant College of Optical Sciences, University of Arizona, 1630 E. University Blvd, Tucson, AZ 85721, USA
[2]Optical Perspectives Group, LLC, 7011 E. Calle Tolosa, Tucson, AZ 85750, USA
[3]Institut National de La Recherche Scientifique, Centre Énergie Matériaux Télécommunications,Varennes, QC, J3XIS2, Canada
[4]ASML US, LP, 77 Danbury Rd, Wilton, CT 06897, USA
*dkim@optics.arizona.edu

Abstract: In this study, we explore the behavior of Bessel beams as they propagate through a misaligned apertured optical system in practice. Based on experimental observations, we propose what we believe to be a novel hypothesis that a Bessel beam propagating through an optical system behaves identically to a paraxial ray under certain conditions. We then derive analytical formulas for the propagation of Bessel beams in Cartesian coordinates and the Huygens-Fresnel principle. Additionally, another simulation employing Gaussian decomposition was conducted, and we compared both simulations with experimental results, demonstrating a high correlation. Our findings indicate that Bessel beams can be interpreted as meridional rays when passing through misaligned spherical surface systems, allowing us to achieve quasi-ray tracing in practice. We further discuss the significance of utilizing this property of Bessel beams for precise optical alignment, highlighting its potential to enhance the accuracy and efficiency of optical systems.

1. Introduction

Bessel functions are exact solutions to the Helmholtz equation [1]. Due to their unique properties, such as being diffraction-free and having an exceptional depth of field (DOF) [2], BGBs are very useful in microscopies through extended DOF to improve temporal resolution and speed up image acquisition in thick volume bio samples [3], ultrasound imaging systems [4], or for free space optical communications to overcome atmospheric turbulence [5].

Nearly 30 years ago, Santarsiero et al. [6] theoretically demonstrated that the Bessel-Gauss beams (BGB) propagated through paraxial optical systems analogous to a meridional ray, we remained skeptical of its conclusion. More recent papers [7–10] explicitly discuss the propagation of BGB through misaligned first-order optical systems but talks about enough variations of the idea that the direct connection between the BGB and a single meridional ray is obscured. There was limited research demonstrating the direct relationship between BGB and optical systems in practice. Until few years back, R. E. Parks et al. [11] experimentally investigated using Bessel beams to measure the straightness of machine tool motions. The ease of creating a Bessel beam with a zone plate grating and optical fiber source and the method's sensitivity led to investigations of using the Bessel beam for optical centering [12]. This use of centering made it seem as if the Bessel beam was propagating through an optical system as if it were a single ray, as used in a lens design program [13]. We realized that if the Bessel beam was strictly analogous to a ray in a design program, then the Bessel beam "ray" could be located experimentally anywhere inside an optical system and anywhere outside well beyond either object or image. This useful feature depended on confirming that there was an explicit connection between Bessel beam propagation and its lens design ABCD meridional ray tracing analog.

#543829 https://doi.org/10.1364/OE.543829
Journal © 2024 Received 18 Oct 2024; revised 26 Nov 2024; accepted 30 Nov 2024; published 20 Dec 2024

Optics EXPRESS

To this end, we used two theoretical methods to simulate BGB propagation and used these models to compare with experimental results of BGB propagation. The first theoretical approach was a MATLAB model of Fresnel propagation [14] of a spherical wavefront through an Axicon. The second was a physical optical ray propagation simulation using the lens design program, Zemax. These two models agreed well and further aligned well with the experimental results described in the final part of the paper. This agreement gives us confidence that we can predict the propagation path of a BGB anywhere throughout an optical system using a real meridional ray from an ABCD description of the system. This leads directly to the usefulness of BGB for optical alignment applications. The exceptional size of the central peak and its non-diffractive nature give BGB a significant advantage over traditional laser beams commonly used in optical alignment. The full width at half maximum (FWHM) of a commercial HeNe laser is on the millimeter scale, whereas using BGB in experiments results in a spot size on the micrometer scale. On the other hand, interferometry is often recommended in precision alignment fields. There is no doubt that interferometry can achieve alignment accuracy on the scale of a wavelength. However, the reality is that interferometry instruments are significantly more expensive than BGB equipment. Additionally, the requirement for a null object in interferometry presents a major limitation, restricting its widespread application in optical alignment testing. In summary, BGB offers greater accessibility for engineers and significantly higher cost efficiency while still providing high alignment accuracy.

2. Experimental setup

According to the paper published by Durnin et al. [15], the Fourier transform of an ideal BGB is a ring, meaning the BGB can be generated by a circular slit aperture [16]. However, idealized BGB cannot be generated experimentally due to the finite size of the aperture [17]. The Bessel beam been generated in practice is called generated Bessel beam, or quasi-Bessel beam (QBB).

To study the effects of misalignment on the propagation of a QBB, we employed a precise test setup. This setup as shown in Fig. 1 was composed of three major components, a QBB generator, a lens holder mounted on an x-y slide, and a Point Source Microscope mounted on a vertical stage as the detector.

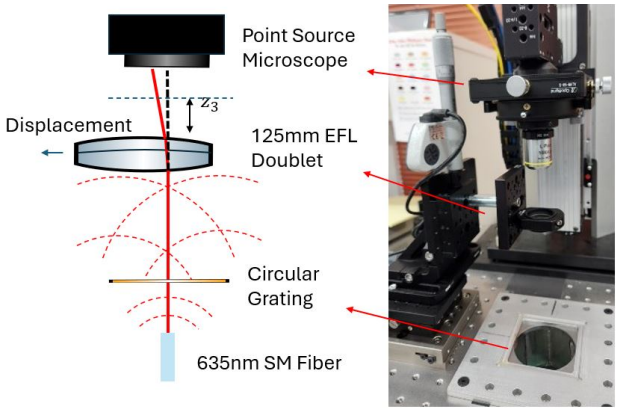

Fig. 1. The figure illustrates the optical setup implementing Bessel beam to study misaligned optical systems. A point source (635nm) illuminates the circular grating probing a lens placed at the focal distance away. The lens is slightly decentered through X-Y translation stage, The Bessel beam as a result deviates and the PSM objective records it's spot, an elaborated version of the PSM is presented to the right.The distance from the fiber to the grating is 205 mm, the distance from the grating to the lens is 125 mm, and the distance from the lens to the observation plane Z_3 is varied to observe the displacement effect of QBB.

Optics EXPRESS

The QBB generator consists of a single mode fiber as the source of 635 nm illumination placed 250 mm behind and centered on a zone plate, a chrome on fused silica grating of concentric circles with 20 μm/lp spacing. This produces a QBB with a convergence angle of approximately ±1.364° close to the grating when illuminated with a spherical wavefront from the source, centered 250 mm behind the grating. The manufacturing errors of the circular grating can be categorized into three main types. First, scaling error occurs when the circular grating is produced with an incorrect spatial frequency. However, this does not affect the displacement of the center peak, as the wave remains rotational symmetric. Second, random errors, such as defective spots on the grating, generally have a negligible impact due to the averaging effect of rotational symmetry and constant interference. Finally, non-symmetric errors could degrade the quality of the Bessel beam. However, with the high standards of modern grating manufacturing, such errors are highly unlikely. In the rare case that such defects occur, the grating can simply be replaced with a higher-quality one. It is important to note that quality of the grating will affect generating QBB, especially in fields such as imaging and lithography. However, in the application of alignment, we rely more on the non-diffracting nature of Bessel beams, which arises from the rotational symmetric structure of the grating. Most manufacturing errors within industrial standards are tolerable in this context.

A lens holder for a 125 mm effective focal length (EFL) doublet attached to an x-y stage equipped with digital micrometers with 1 μm resolution was used to center the lens on the QBB. The stage was then used to decenter the lens during the measurements of beam deviation versus the height of the detector. The lens was 125 mm above the grating when mounted in the holder.

The detector we utilized was a Point Source Microscope (PSM) [18], a contemporary autostigmatic microscope mounted on a motorized vertical stage with an encoder with 1 μm resolution and 900 mm of travel. The PSM was used not only as a video microscope during the measurements but also in its autostigmatic mode to align the single-mode fiber on the axis of the zone plate grating. The vertical stage scale was set to zero when the PSM was focused on the upper surface of the lens.

Before measuring the beam deviation due to the lens decentration, the QBB divergence was measured as a function of height above the grating with no lens in the holder. Then, the lens was inserted into the holder for the deviation measurements. Since the vertical stage is not perfectly straight nor perfectly aligned to the QBB, the deviation measurements were made by moving the lens equal distances from the nominal x-y stage zero and measuring the total motion of the QBB as the lens was moved from one extreme to the other. This eliminated errors due to shortcomings of the vertical stage.

3. Theoretical modeling

In this section, we derive the equation for generating a Bessel beam as it propagates through an optical system.

3.1. Quasi-Bessel beams

There are many different methods been proposed to create QBB [19–21]. In our approach, we generate QBB using a grating of concentric, equally spaced circles [22],which is equivalent to an axicon [23]. Using a circular grating instead of an axicon is primarily due to the challenges associated with the fabrication process. The optical path difference (OPD) mapped in the axicon plane can be expressed by:

$$\mathrm{OPD}(x, y) = n \times \Delta(x, y) + n_0 \times [\Delta_0 - \Delta(x, y)] \tag{1}$$

where n is the refractive index of the axicon, n_0 is the refraction index of the free space. Δ_0 is a constant related to the thickness of the axicon, and $\Delta(x, y)$ can be written as Eq. (2), in which α is

Optics EXPRESS

the base angle for the cross-section of the axicon.

$$\Delta(x, y) = \Delta_0 - \sqrt{x^2 + y^2} \times \tan(\alpha) \tag{2}$$

With the phase map of the axicon known, we can now express the wave equation at the plane (x_2, y_2) at a distance z_2 from the axicon as follows:

$$\begin{aligned} u_2'(x_2, y_2) = & \frac{e^{jkz_2}}{j\lambda z_2} \times \frac{e^{jkz}}{j\lambda z} \\ & \times \iint P(x, y) \times e^{jk(n\Delta(x,y)+n_0[\Delta_0-\Delta(x,y)])} \\ & \times e^{\frac{j\pi}{\lambda z}(x^2+y^2)} \times e^{\frac{j\pi}{\lambda z_2}((x_2-x)^2+(y_2-y)^2)}\, dx\, dy \end{aligned} \tag{3}$$

where $P(x, y)$ is the aperture function, and it is circular in the case. In our experiment, we used a single mode fiber as the source, which is considered as a point source to generate perfect spherical wavefront. In Eq. (3), we used z to represent the distance a spherical wavefront propagates from the source to the axicon. We define:

$$u_l'(x, y) = P(x, y) \times e^{jk(n\Delta(x,y)+n_0[\Delta_0-\Delta(x,y)])} \times e^{\frac{j\pi}{\lambda z}(x^2+y^2)} \tag{4}$$

With simplification, the $u_2'(x_2, y_2)$ can be expressed in terms of Fourier transformations:

$$\begin{aligned} u_2'(x_2, y_2) &= \frac{e^{jkz_2}}{j\lambda z_2} \times \frac{e^{jkz}}{j\lambda z} \iint u_l'(x, y)\, e^{\frac{j\pi}{\lambda z_2}(x_2^2+y_2^2+x^2+y^2-2(xx_2+yy_2))}\, dx\, dy \\ &= \frac{e^{jkz_2}}{j\lambda z_2} \times \frac{e^{jkz}}{j\lambda z} \times e^{\frac{j\pi}{\lambda z_2}(x_2^2+y_2^2)} \iint u_l'(x, y)\, e^{\frac{j\pi}{\lambda z_2}(x^2+y^2)}\, e^{\frac{j2\pi}{\lambda z_2}(xx_2+yy_2)}\, dx\, dy \\ &= \frac{e^{jkz_2}}{j\lambda z_2} \times \frac{e^{jkz}}{j\lambda z} \times e^{\frac{j\pi}{\lambda z_2}(x_2^2+y_2^2)} \mathcal{F}_2\left(u_l'(x, y)\, e^{\frac{j\pi}{\lambda z_2}(x^2+y^2)}\right)_{\xi=\frac{x_2}{\lambda z_2}, \eta=\frac{y_2}{\lambda z_2}} \end{aligned} \tag{5}$$

The expression of $u_2'(x_2, y_2)$ indicates the magnification relationship between the axicon plane and the observation plane, allowing us to compute the intensity profile at various propagation distances. Figure 2 demonstrates the intensity profile of the observation plane located 281 mm away from the axicon. In Fig. 3, we introduce another simulation from Zemax, which is based on Gaussian decomposition, and we compared simulations with our experimental result. In the centroid range, both simulations show a high degree of correlation with experimental observations; however, the correlation decreases at the edge of the plot since the simulations are based on the approximation of small angles, and this approximation is less valid with a large Field of View (FOV). Despite the edge effect in the simulation, we can confidently state that our simulation achieves a high degree of accuracy in the range of interest.

Unlike idealized BGB, QBB does not maintain its intensity distribution throughout propagation, meaning that the QBB will eventually vanish.The on-axis irradiance distribution of QBB has been comprehensively studied by Dong and Pu [24], and Cai and Lü [7] have also investigated the off-axis irradiance distribution.The amplitude distribution of BGB and QBB at the optical output planes in a matrix formulation is also provided by Belafhal et al. [25] Therefore, this article will not delve into a detailed illustration of these topics. Nevertheless, despite the intensity variation during propagation, we observed that the QBB retain its Bessel function profile in a uniform medium, with the only change being the scaling of the J_0 function. In our experiment, we observed a distinct pattern of the QBB after 900 mm of propagation, with the FWHM of the peak consistently remaining below 60 μm. This extended propagation distance is more than sufficient for the alignment requirements of most commercial optical systems.

Optics EXPRESS

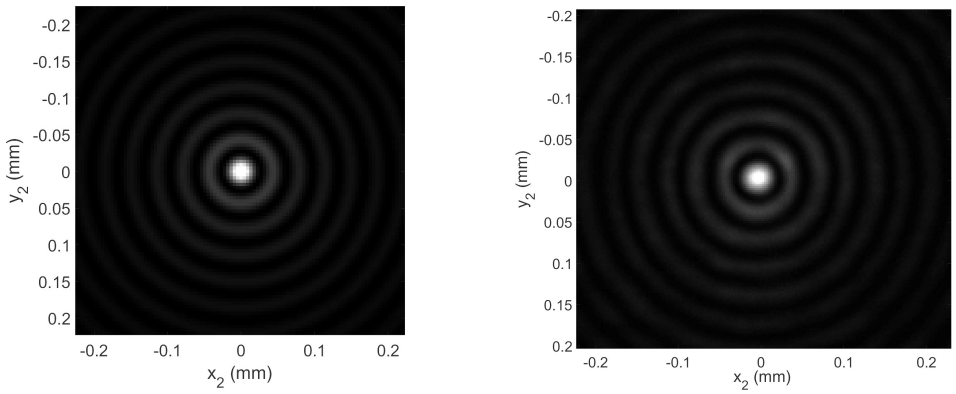

(a) Wave propagation simulation (b) Experimental observation

Fig. 2. A 2-D intensity plot from Fresnel Propagation simulation and reference observation from experiment at the same propagation distance at 281 mm. The comparison of these images is evaluated by analyzing the *x*-cross section through the central peak, and the cross section shows a high degree of matching in the observations.

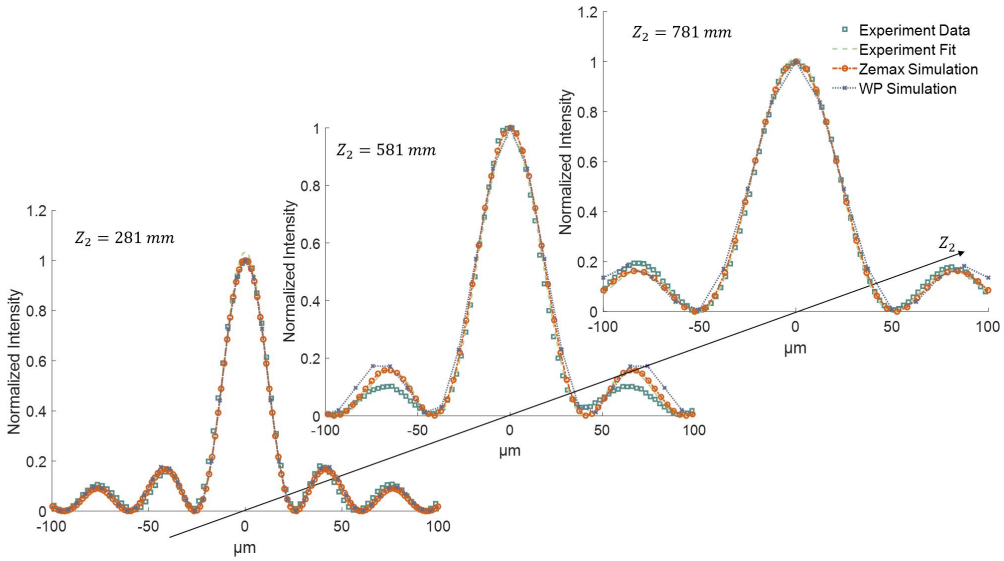

Fig. 3. Comparison of wave propagation and Zemax simulation results with experimental data for three positions of the observation plane Z_2= 281, 581, 781 mm. These intensity profiles are observed with QBB generated by a circular grating and propagated over different distances Z_2. A strong agreement is found for the central peak in all three situations.

Our observation aligns with the research published by Halba et al. [26], which discusses QBB numerically as they propagate through an ABCD system. Their research suggests that QBB can be analyzed using the ABCD matrix specifically on axis. In this article, we study the paraxial behavior of QBB from a different perspective, focusing on the peak location rather than the scaling factor of the beam for optical alignment purpose.

Optics EXPRESS

3.2. QBB through optical elements

After generating QBB with an axicon, we want to explore their behavior as they propagate through an optical system, particularly under conditions of misalignment. From the principles of Fresnel propagation, we understand that a wave passing through an optical element, such as a lens, can be described by the wavefront multiplied by the phase map of the lens. At a distance z_3 from the rear principle point of the lens, the phase u_3' been observed can be expressed as:

$$u_3'(x_3, y_3) = \frac{e^{jkz_3}}{j\lambda z_3} \times e^{\frac{j\pi}{\lambda}\left(\frac{1}{z_3}-\frac{1}{f}\right)(x_3^2+y_3^2)} \mathcal{F}_2\left(u_2'(x_2, y_2) \times e^{\frac{j\pi}{\lambda}\left(\frac{1}{z_3}-\frac{1}{f}\right)(x_2^2+y_2^2)}\right)_{\xi=\frac{x_3}{\lambda z_3}, \eta=\frac{y_3}{\lambda z_3}} \tag{6}$$

It is not surprising to observe that the QBB, after propagating through an optical system, maintains a high correlation with the Bessel function. The simulation demonstrates that the Fourier transform of a Bessel function, when multiplied by the Fresnel propagation term, continues to exhibit Bessel function characteristics. To assess the reliability of our simulation, we recorded the QBB propagation through the lens with EFL=125mm at intervals from 10 mm to 130 mm. A schematic drawing of this setup is demonstrated at Fig. 1. From Fig. 4, the comparison between the simulation and experimental data reveals a noticeable deviation when using the wave propagation method. This discrepancy is primarily due to the use of a phase map instead of an actual lens in the wave propagation calculations. However, despite this approximation, the deviation is comparable to the reading error, suggesting that the simulation remains reasonably accurate.

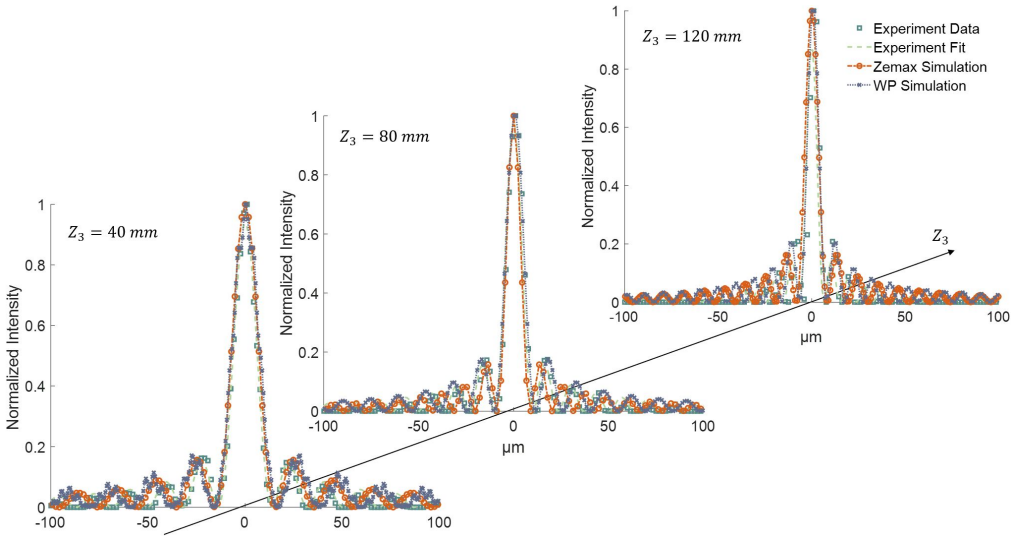

Fig. 4. Comparison of wave propagation and Zemax simulation results with experimental data for three positions of the observation plane Z3 = 40, 80, 120 mm. These intensity profiles are observed with QBB generated by a circular grating, propaged by distance of 125mm in free space, propgate through a lens and observed in distance of Z_3.The set up is same deomstrated by Fig. 1. A strong agreement is found for the central peak in all three situations where a max error between WP an experimental for the FWHM of center peak of 2.3 um is observed in the case of Z3= 80mm.

Optics EXPRESS

3.3. QBB through misaligned optical elements

In optical alignment, tilting and displacement are the two major categories of misalignment. The simulation method for both involves applying the misalignment to the lens coordinates. For the purposes of this article, we will focus on displacement simulation to demonstrate our approach.

To introduce decentering into the system, we add a decentering term, Δx_2, into the equation. It is crucial to correctly recover the coordinates, so we need to subtract Δx_2 from x_3 to ensure that the observation plane aligns with the global coordinate system. This adjustment allows us to accurately analyze the effects of decentering on the QBB and maintain consistency in our measurements.

The decentering result of QBB is recorded in Table 1, and the data clearly indicates that the wave propagation method is nearly identical to a single ray passing through a decentered paraxial lens, with less than 0.1% difference. This is an exciting discovery because QBB exhibit unique stability compared to other beams. They maintain a high correlation with a Bessel function, with the central spot size remaining unchanged even under decentering up to 0.5 mm. This demonstrates the invariance of the scaling factor for QBB, highlighting their robustness and potential applications in optical systems.

Table 1. A lens is decentered with respect to the optical axis by the amount shown in column 1. Comparison of decentering results from wave propagation method and ray tracing through both paraxial and actual lenses. The observation plane is 70 mm from the rear side of the lens. A high correlation is observed between the QBB decentering obtained from the simulation and that predicted by ray tracing with a paraxial lens.

Decentering (mm)	Zemax (thick lens) (mm)	Zemax (paraxial) (mm)	QBB simulation (mm)
0.1	0.0569	0.0550	0.0550
0.2	0.1138	0.1121	0.1121
0.3	0.1706	0.1683	0.1683
0.4	0.2275	0.2240	0.2236
0.5	0.2844	0.2790	0.2788

The discrepancy between the paraxial lens and the thick lens ray tracing can be easily compensated by basic geometrical optics calculations. This means that simulations show QBB passing through an optical element with an acceptable range of decentering behave very similarly to ideal paraxial rays. To test our hypothesis, we collected more experimental data by changing the observational plane distance. The result is shown in Fig. 5.

The determination coefficient, R^2, represents the accuracy of the chief ray trace from the Zemax simulation when compared to the shifted experimental data. For instance, in the 90 mm observation distance trial, the lens decentering, based on measurements, is -9.078 μm. With all data points shifted by 9.078 μm, the R^2 value exceeds 0.999, indicating an exceptionally high degree of correlation between the experimental data and the ray tracing simulation. This strong correlation provides compelling evidence that the QBB behaves almost identically to a paraxial ray. The root mean square error (RMSE) estimated from each trial are 1.173 μm, 1.410 μm, and 1.954 μm, which can be converted to angular errors of 3.457 arcsec, 3.636 arcsec, and 4.030 arcsec, respectively. This degree of alignment accuracy is sufficient for most commercial optics and significantly simplifies the alignment procedure compared to interferometry.

Up to this point, we have provided evidence that QBB exhibits characteristics similar to paraxial rays in theoretical calculations and experimental observations. This means that anyone using QBB for alignment can utilize the ABCD matrix approach for misalignment calculations, instead of relying on complex wave propagation simulations. Now that we have theoretical verification that a Bessel beam propagates through an optical system as though it were a single ray that can be described in the paraxial region of a lens by ABCD matrix optics, the study of optical alignment

Optics EXPRESS

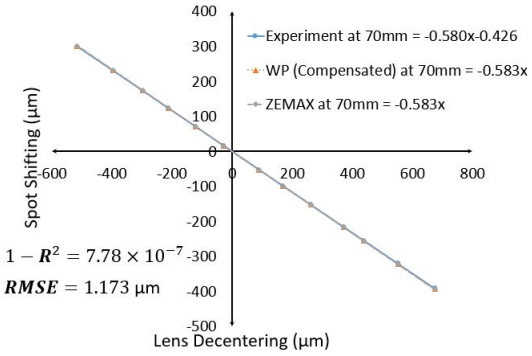

(a) Observation plane at 70 mm

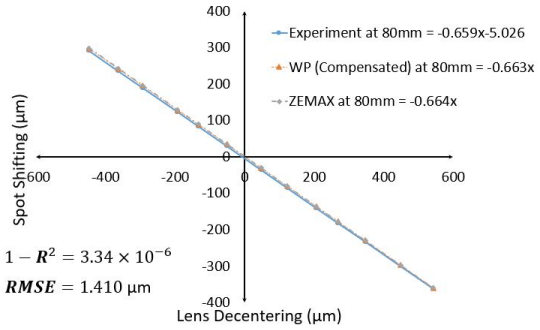

(b) Observation plane at 80 mm

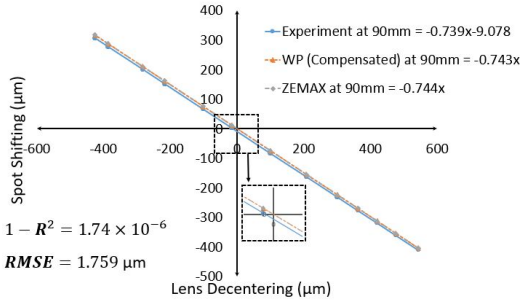

(c) Observation plane at 90 mm

Fig. 5. Linear fit for both simulation and experiment data with various propagation distance. A high correlation is observed in the plot, providing strong evidence that the QBB is displaced nearly identically to a paraxial ray in misaligned optics. In (c), the experimental data intercept the y-axis not at the origin, indicating that the lens is misaligned by a degree on the order of arcseconds.

and how to perform alignment becomes much simpler. Optical and optomechanical engineers with no lens design experience can model the effects of misalignment as they go about their functions of designing lens mounts and alignment fixtures without having to go back to the lens designer. This direct and quantitative measurement of misalignment gives the engineers greater control over the alignment process.

Optics EXPRESS

4. Lens alignment procedure with QBB

By applying the quasi-beam property of the QBB, an experiment was conducted to demonstrate one of the configurations in which the QBB can be utilized to align optical elements in practice. In the setup shown in Fig. 6, the alignment process involves the use of the PMS, which serves both as a point light source and as an observation tool for the QBB. The source illuminates through the lens, allowing observation of the reflected ray from one of the lens surfaces.

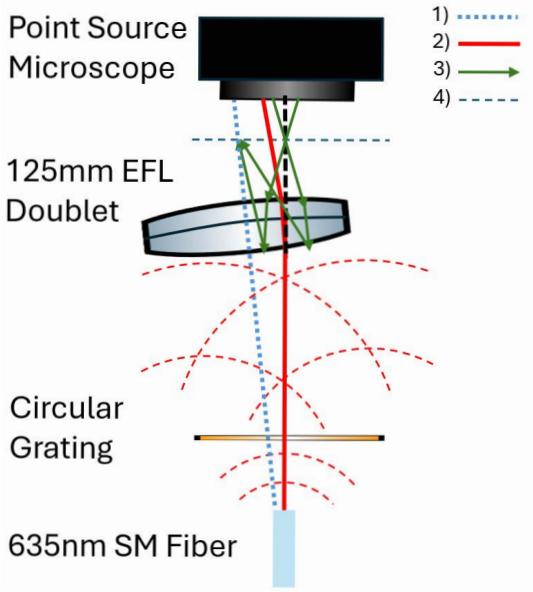

Fig. 6. Schematic diagram of the QBB and PSM combination for lens alignment. The labeled lines represent, in descending order: 1) optical axis of the lens, 2) center peak of the QBB, 3) illumination from the PSM, and 4) the focal plane of the objective.

The alignment procedure begins with aligning the PSM with the QBB, where the center of the first-order peak is marked as the reference crosshair. Subsequently, a lens is inserted in the beam path, resulting in two observable spots at the detector plane as shown in Fig. 7 : the first is the deviated QBB, and the second is the reflected spot from the lens surface, representing the optical center of curvature.

The iterative alignment process is straightforward and converges rapidly. Initially, the lens is decentered to align the QBB with the crosshair. Following this, the lens is tilted to bring the reflected spot from the optical center of curvature into alignment with the crosshair. Since tilting the lens can slightly decenter the beam, it is necessary to repeat the decentering and tilting steps iteratively. Typically, alignment is achieved within three to four iterations, resulting in a precision better than 1 μm for decentering and in scale of arcseconds for tilt, which mainly depends on the set up configuration and microscope resolution, ensuring that both light spots are aligned to pass through the microscope objective.

Once the lens is aligned, the QBB should be coaxial with the optical axis of the lens, and both spots should coincide with the crosshair. Figure 8 presents the iterative convergence observed during experimental alignment. The absolute distance are calculated from the crosshair to the peak of points.

In conclusion, this experiment demonstrates that a lens can be aligned in several iterations using the QBB and PSM combination with high precision. The accuracy of this alignment is ultimately limited only by the resolution of the PSM. For a multi-lens system, using the same

Optics EXPRESS

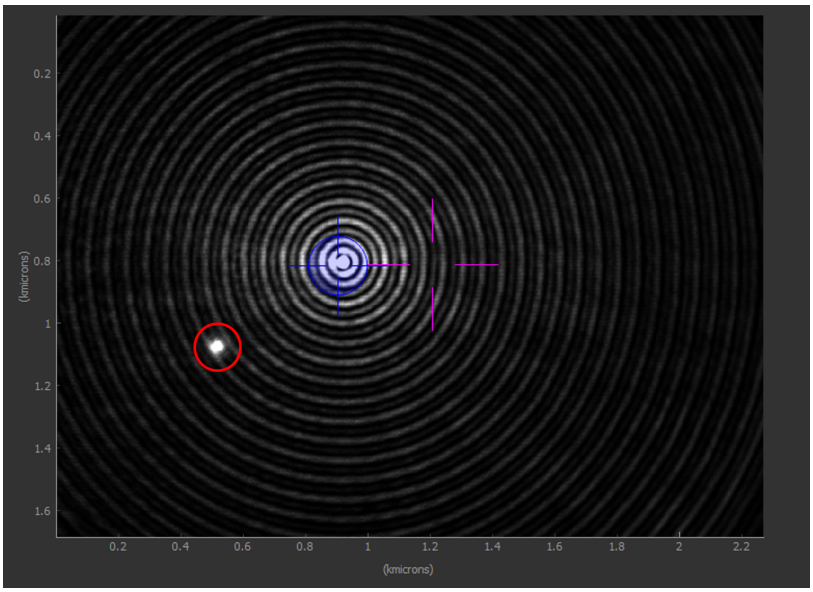

Fig. 7. Captured user interface from PSM: the bright spot in the red circle indicates the optical center of curvature which is measured as the focused beam reflected from PSM; the blue crosshair indicates the center of QBB, and the light pink crosshair indicates the location of the reference optical axis, which is defined before insert any lens in between lens and circular grating. The PSM is placed 24.5 mm away from the flat surface of a plano-convex lens with a 50.2 mm EFL, and the circular grating is placed 780 mm away from the lens on the opposite side. The misalignment of the lens with respect to the QBB results in a displacement between the reference crosshair, the center of the QBB, and the reflected beam from the PSM.

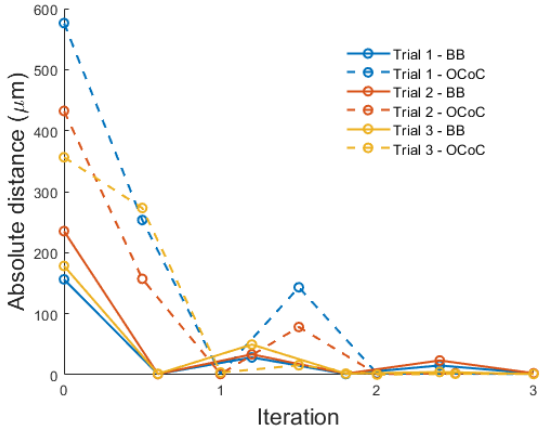

Fig. 8. Recorded the distance from the reference crosshair for both the QBB spot and the optical center of curvature (OCoC) while aligning a 50.2 mm EFL lens. The lens was initially randomly misaligned. The displacement of the lens is first applied to align the QBB with the crosshair, and then tip/tilt is adjusted to align the OCoC with the crosshair, which is defined as one iteration. These iterations are repeated three times, and two of the spots can be aligned with the reference within the resolution limit of the PSM.

Optics EXPRESS

procedure, lenses can be added sequentially, and the QBB through the previously aligned lenses can still serve as the reference optical axis of the system. Of course, this is not the only scenario in which the QBBs can be applied for optical alignment. For instance, by combining an axicon grating with the PSM, a QBB-based autocollimator can be developed. Due to its exceptionally small central peak size, the QBB autocollimator offers significant advantages, allowing it to be applied to a wider range of optics and simplify the step of seeking the focal spot with zoom lens. Additionally, the QBB can be combined with linear gratings to construct multiple QBBs that emulate multiple quasi-rays through an optical system. This approach enables the decoupling of misalignment and allows extracting more information from the optical system.

5. Conclusion

In summary, we investigated the propagation of QBB through a misaligned optical system and derived analytical formulas based on the Huygens-Fresnel principle. Our findings showed a high correlation between experimental observations, simulations, and ray-tracing results, validating our hypothesis that QBB behaves similarly to paraxial rays when propagating through a misaligned apertured system. With this hypothesis confirmed, we discussed the significance of QBB properties in optical alignment. Our results indicate that the use of QBB for optical alignment can achieve micron and arcsecond-level precision, establishing it as a convenient and effective method for optical alignment. It is important to note that we only discussed spherical surfaces in this experiment, which sets a limitation for our hypothesis. Nevertheless, preliminary experimental data indicates that QBB can also be effective in aligning aspherical reflective optical elements, as demonstrated in our previous research with a parabolic mirror [27]. In our further studies, our team will focus on exploring the boundaries of this hypothesis within more complex optical systems.

Disclosures. The authors declare no conflict of interest.

Data availability. Data underlying the results presented in this paper are not publicly available at this time but may be obtained from the authors upon reasonable request.

References

1. J. Durnin, "Exact solutions for nondiffracting beams. i. the scalar theory," J. Opt. Soc. Am. A **4**(4), 651–654 (1987).
2. S. Khonina, N. Kazanskiy, S. Karpeev, *et al.*, "Bessel beam: Significance and applications-a progressive review," Micromachines **11**(11), 997 (2020).
3. G. Thériault, Y. Koninck, and N. McCarthy, "Extended depth of field microscopy for rapid volumetric two-photon imaging," Opt. Express **21**(8), 10095 (2013).
4. D. Hsu, F. Margetan, and D. Thompson, "Bessel beam ultrasonic transducer: Fabrication method and experimental results," Appl. Phys. Lett. **55**(20), 2066–2068 (1989).
5. P. Birch, I. Ituen, R. Young, *et al.*, "Long-distance Bessel beam propagation through kolmogorov turbulence," J. Opt. Soc. Am. A **32**(11), 2066 (2015).
6. M. Santarsiero, "Propagation of generalized Bessel-Gauss beams through ABCD optical systems," Opt. Commun. **132**(1-2), 1–7 (1996).
7. Y. J. Cai and X. Lü, "Propagation of Bessel and Bessel-Gaussian beams through an unapertured or apertured misaligned paraxial optical systems," Opt. Commun. **274**(1), 1–7 (2007).
8. C. Zhao, L. Wang, X. Lu, *et al.*, "Propagation of high-order Bessel-Gaussian beam through a misaligned first-order optical system," Opt. Laser Technol. **39**(6), 1199–1203 (2007).
9. M. X. Shen, S. M. Wang, and D. M. Zhao, "Propagation of flattened Gaussian beams passing through a misaligned optical system with finite aperture," Optik **115**(5), 193–196 (2004).
10. G. L. Ding and B. D. Lü, "Generalized Huygens-Fresnel diffraction integral for misaligned asymmetric first-order optical systems and decentered anisotropic Gaussian Schell-model beams," J. Opt. Soc. Am. **19**(3), 485–490 (2002).
11. R. E. Parks, "Computer generated holograms as 3-dimensional calibration artifacts," in *Proc. ASPE Annual Meeting*, (2017).
12. R. E. Parks, "Alignment using axicon plane gratings," Proc. SPIE **10747**, 1074703 (2018).
13. R. E. Parks and D. Kim, "Physical ray tracing with Bessel beams," in *Proc. of ASPE Spring Topical Meeting*, (Tucson, AZ, 2023).
14. J. W. Goodman, *Introduction to Fourier Optics* (Macmillan Learning, 2017), 4th ed.
15. J. Durnin, J. Miceli, and J. Eberly, "Diffraction-free beams," Phys. Rev. Lett. **58**(15), 1499–1501 (1987).
16. K. Khare, *Fourier Series and Transform* (John Wiley & Sons, Ltd, 2015), chap. 2, pp. 19–47.

Optics EXPRESS

17. O. Brzobohatý, T. Cižmár, and P. Zemánek, "High quality quasi-Bessel beam generated by round-tip axicon," Opt. Express **16**(17), 12688–12700 (2008).
18. O. P. Groups, "Point source microscope," (2016).
19. C. Palma, "Decentered Gaussian beams, ray bundles, and Bessel-Gauss beams," Appl. Opt. **36**(6), 1116–1120 (1997).
20. P. Overfelt, "Generation of a Bessel-Gauss pulse from a moving disk source distribution," J. Opt. Soc. Am. A **14**(5), 1087–1091 (1997).
21. A. S. Rao, "A conceptual review on Bessel beams," Phys. Scr. **99**(6), 062007 (2024).
22. R. E. Parks, "Practical considerations for using grating produced Bessel beams for alignment purposes," Proc. SPIE **11816**, 11–18 (2021).
23. S. N. Khonina, N. L. Kazanskiy, P. A. Khorin, *et al.*, "Modern types of axicons: New functions and applications," Sensors **21**(19), 6690 (2021).
24. M. Dong and J. Pu, "On-axis irradiance distribution of axicons illuminated by a spherical wave," Opt. Laser Technol. **39**(6), 1258–1261 (2007).
25. A. Belafhal and L. Dalil-Essakali, "Collins formula and propagation of Bessel-modulated Gaussian light beams through an ABCD optical system," Opt. Commun. **177**(1-6), 181–188 (2000).
26. E. M. El Halba, M. Boustimi, L. Ez-zariy, *et al.*, "Propagation characteristics of Bessel-like beams through ABCD optical system," Opt. Quantum Electron. **49**, 1–11 (2017).
27. R. E. Parks, "Aligning reflecting optics with bessel beams," Proc. SPIE **11488**, 114880J (2020).